NPTC-NET: NARROW-BAND PARALLEL TRANSPORT CONVOLUTIONAL NEURAL NETWORK ON POINT CLOUDS

Anonymous authors
Paper under double-blind review

ABSTRACT

Convolution plays a crucial role in various applications in signal and image processing, analysis and recognition. It is also the main building block of convolution neural networks (CNNs). Designing appropriate convolution neural networks on manifold-structured point clouds can inherit and empower recent advances of CNNs to analyzing and processing point cloud data. However, one of the major challenges is to define a proper way to "sweep" filters through the point cloud as a natural generalization of the planar convolution and to reflect the point cloud's geometry at the same time. In this paper, we consider generalizing convolution by adapting parallel transport on the point cloud. Inspired by a triangulated surface based method Schonsheck et al. (2018), we propose the Narrow-Band Parallel Transport Convolution (NPTC) using a specifically defined connection on a voxelized narrow-band approximation of point cloud data. With that, we further propose a deep convolutional neural network based on NPTC (called NPTC-net) for point cloud classification and segmentation. Comprehensive experiments show that the proposed NPTC-net achieves similar or better results than current state-of-the-art methods on point clouds classification and segmentation.

1 INTRODUCTION

Convolution is one of the most widely used operators in applied mathematics, computer science and engineering. It is also the most important building block of Convolutional Neural Netowrks (CNNs) which are the main driven force in the recent success of deep learning LeCun et al. (2015); Goodfellow et al. (2016).

In the Euclidean space $\mathbb{R}^n$, the convolution of function f with a kernel (or filter) k is defined as

$$(f * k)(x) := \int_{\mathbb{R}^n} k(x-y)f(y)dy. \tag{1}$$

This operation can be easily calculated in Euclidean spaces due to the shift-invariance of the space so that the translates of the filter k, i.e. $k(x-y)$ is naturally defined. With the rapid development of data science, more and more non-Euclidean data emerged in various fields including network data from social science, 3D shapes from medical images and computer graphics, data from recommending systems, etc. Therefore, geometric deep learning, i.e. deep learning of non-Euclidean data, is now a rapidly growing branch of deep learning Bronstein et al. (2017). In this paper, we will discuss how we can generalize the definition of convolution to (manifold-structured) point clouds in a way that it inherits desirable properties of the planar convolution, thus it enables to design convolutional neural networks on point clouds.

One of the main challenges of defining convolution on manifolds and point clouds (a discrete form of manifolds) is to define translation $x - y$ on the non-Euclidean domain. Other than convolutions, we also need to properly define pooling to enable networks to extract global features and to save memory during training. Multiple types of generalization of convolutions on manifolds, graphs and point clouds have been proposed in recent years. We shall recall some of them and discuss the relation between existing definitions of convolutions and the proposed narrow-band parallel transport convolution.

1.1 Related Work of Convolutions on Non-Euclidean Domains

Spectral methods avoid the direct definition of translation $x - y$ by utilizing the convolution theorem: for any two functions f and g, $\widehat{f * g} = \hat{f} \cdot \hat{g}$. Therefore, we have $f * g = (\hat{f} \cdot \hat{g})^{\vee}$, where $\wedge$ and $\vee$ represent generalized Fourier transform and inverse Fourier transform provided through the associated Laplace-Beltrami (LB) eigensystem on manifolds. To avoid computing convolution through full eigenvalue decomposition, polynomial approximation is proposed and yields convolution as action of polynomials of the LB operator Hammond et al. (2011); Dong (2017). Thus, convolutional neural networks can be designed Bruna et al. (2014); Defferrard et al. (2016); Levie et al. (2019). Spectral methods, however, suffer two major drawbacks. First, these methods define convolution in the frequency domain. As a result, the learned filters are not spatially localized. Secondly, spectral convolutions are domain-dependent as deformation of the ground manifold will change the corresponding LB eigensystem. This obstructs the use of learning networks from one training domain to a new testing domain Schonsheck et al. (2018).

Spatial mesh-based methods are more intuitive and similar to the Euclidean case, and this is one of the reasons why most of the existing works fall into this category. The philosophy behind these methods is that the tangent plane of a 2-dimensional manifold is embedded to a 2-dimensional Euclidean domain where convolution can be easily defined. In this paper, we make the first attempt to interpret some of the existing mesh-based methods in a unified framework. We claim that most of the spatial mesh-based methods can be formulated as

$$(f * k)(x) := \int_{\mathcal{T}_{x,\epsilon}\mathcal{M}} k(\phi(x, v)) f(v) \mathrm{d}v, \quad x \in \mathcal{M}. \tag{2}$$

Here, $k : \mathbb{R}^2 \to \mathbb{R}$ is a convolution kernel and $\mathcal{T}_{x,\epsilon}\mathcal{M} = \{v \in \mathcal{T}_x\mathcal{M} : \langle v, v \rangle_{g_x} \leq \epsilon^2\}$ with $\epsilon > 0$ being the size of the kernel. The mapping $\phi(x, v) : \mathcal{M} \times \mathcal{T}_x\mathcal{M} \to \mathbb{R}^2$ is defined as

$$\phi(x, v) = (\alpha_1, \alpha_2) = \left(\left\langle v, \vec{u}_x^1 \right\rangle_{g_x}, \left\langle v, \vec{u}_x^2 \right\rangle_{g_x} \right), \tag{3}$$

where $\vec{u}_x^j \in \mathcal{T}_x\mathcal{M}$, $j = 1, 2$. For simplicity, we will denote $\vec{u}_x = (\vec{u}_x^1, \vec{u}_x^2)$. Most of the designs of the existing manifold convolutions focused on the designs of $\vec{u}_x$. We remark that possible singularities will lead to no convolution operation at those points. These are isolated points on a closed manifold and do not effect experiment results. In addition, singularities from a given vector field can be overcome using several pairs of vector fields and pooling Schonsheck et al. (2018).

For example, GCNN Masci et al. (2015) and ACNN Boscaini et al. (2016) construct a local geodesic polar coordinate system on a manifold, formulating the convolution as

$$(f * k)(x) = \int k\left((\phi \circ \psi)(\theta, r)\right) (\mathcal{Q}_x f)(r, \theta) \mathrm{d}r \mathrm{d}\theta,$$

where $\mathcal{Q}$ is a local interpolation function with interpolation domain an isotropic disc for GCNN and an anisotropic ellipse for ACNN. A local geodesic polar coordinate system on a manifold can also be transformed to a 2-dimensional planar coordinate system on its tangent plane. Such transformation is the mapping ψ which is defined by the inverse exponential map: $v = exp^{-1}(z(\theta, r))$ with $z(\theta, r)$ being a point in the local geodesic polar coordinate system at $x \in \mathcal{M}$ with coordinates (θ, r). With this, we can easily interpret ACNN within the framework of (2). Indeed, ACNN essentially chooses $\vec{u}_x$ as the directions of the principal curvature at point x. For GCNN, on the other hand, it avoids choosing a specific vector field on the manifold by taking max-pooling among all possible directions of $\vec{u}_x^1$ at each point. Such definition of convolution, however, ignores the correspondence of the convolution kernels at different locations.

The newly proposed PTC Schonsheck et al. (2018) defines convolution directly on the manifold, while uses tangent planes to transport kernels by a properly chosen parallel transport. PTC can be equivalently cast into the form of (2) using the inverse exponential map, and implementation of the proposed parallel transported is realized through choosing specific vector fields $\{\vec{u}_x^j\}_{x \in \mathcal{M}}, j = 1, 2$ guided by a Eikonal equation for transforming vectors along geodesic curves on manifolds.

Spatial point-based methods have wider applications due to their weaker assumptions on the data structure, a point cloud $\mathcal{P} = \{x_i \in \mathbb{R}^3 : i = 1, \ldots, N\} \subset \mathbb{R}^3$ consists of points in a 3-dimensional Euclidean space with the coordinates of the points as the only available information. Manifolds

can be approximated by point clouds via sampling. Computing k-nearest neighborhoods of x or neighbors within a fixed radius can easily convert a point cloud to a local graph or mesh. This is why point cloud is simple, flexible and attracts much attentions lately.

There are mainly two types of point-based convolution. The first type is to combine the information of points directly. These methods can be formulated as

$$(f * k)(x_i) := \sum_{x_j \in \mathcal{N}(x_i)} k(x_i, x_j) f(x_j), \tag{4}$$

where $\mathcal{N}(x_i) \subset \mathcal{P}$ is a neighborhood of x_i and kernel k takes different forms in different methods. PointNet Qi et al. (2017a) is an early attempt to extract features on point cloud. PointNet is a network structure without convolution, or alternatively we can interpret the convolution defined by PointNet has the simplest kernel $k(x_i, x_j) = \delta(x_i, x_j)$ where δ is the Kronecker-Delta. Various later works attempt to improve PointNet by choosing different forms of the kernel k. For example, PointNet++ Qi et al. (2017b) introduces a max pooling among local points, i.e. choosing kernel k as an indicator function: $k(x_i, x_j) = I_{x_j = \arg\max_{z \in \mathcal{N}(x_i)} f(z)}$. Pointcnn Li et al. (2018b) chooses $k(x_i, \cdot) = \beta' A_{x_i}$ where $\beta \in \mathbb{R}^K$ and $A_{x_i} \in \mathbb{R}^{K \times K}$ are trainable variables with $K = |\mathcal{N}(x_i)|$. DGCNN Wang et al. (2018c) proposes an "edge convolution" that can be viewed as fixing $f(x_j) \equiv 1$ and $k(x_i, x_j)$ =MLP$(f(x_i), f(x_i) - f(x_j))$, where MLP means the Multi-Layer Perceptron.

The second type of convolution is defined by first projecting the point cloud locally on an Euclidean domain and then employ regular convolution. This type of methods can also be formulate as (2). For example, Tangent convolutions Tatarchenko et al. (2018) define kernels on the tangent plane, and use 2 principal directions of a local PCA as $\vec{u}_x$. Pointconv Wu et al. (2018) constructs local kernels by interpolation in $\mathbb{R}^3$, i.e. letting $\phi(x, v) = x - v$ which is essentially a local Euclidean convolution.

1.2 The Proposed Convolution: NPTC

In this paper, we propose Narrow-Band Parallel Transport Convolution (**NPTC**), which is a geometric convolution based on point cloud discretization of a manifold parallel transport defined in a specific way. As we observed in the previous section, convolutions in many methods can be written in the form of (2) and (3), while the differences mostly lie in the choices of the vector field $\{\vec{u}_x\}_{x \in \mathcal{M}}$. As observed by Schonsheck et al. (2018) that choosing the vector field properly, the associated convolution can be interpreted as parallel transporting the kernels using the parallel transport associated to the prescribed vector field. The formal definition of parallel transport and connection will presented in Section 2 and detailed descriptions on NPTC will be given in Section 3.

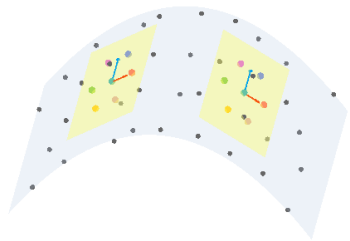

Figure 1: Narrow-band parallel transport convolution on point cloud: black and blue points are sample points of the surface (blue). Each kernel (colored dots) is defined on the tangent plane (yellow). The vectors on the tangent planes that are of the same color are in parallel.

We attempt to define geometric convolutions that can be viewed as translating kernels on the point cloud in a parallel fashion. One naive approach to extend mesh based methods to point cloud is to generate a triangulated surface based on the point cloud. However, this is not as convenient as working directly with the point cloud since in practice not every point cloud corresponds to a legitimate parameterized surface and pooling is not as easy to implement on triangulated surfaces as on point clouds. In addition, it is time-consuming to construct meshes on point clouds. When applied in practice, mesh construction time may be much longer than inference time of some methods directly applied on the point cloud. To avoid mesh constuction and to handle point clouds data directly, we propose to define convolution on point clouds by combining voxelization and geometric convolution.

Now, we describe how NPTC is computed on point clouds. Firstly, point clouds are approximated by voxelization with appropriate resolution, and the vector field $\{\vec{u}_x\}_{x \in \mathcal{M}}$ is defined as the projections of the gradient field of a narrow-band-based distance function on the approximated tangent plane

of the point cloud. Such definition of the vector field is robust to noise, since if the distortion of the coordinates of the points by noise does not exceed the width of the narrowband, the computed gradient field of the distance function in the narrowband remains unchanged. After the vector field $\{\vec{u}_x\}_{x\in\mathcal{M}}$, we use local PCA to estimate normal vectors on the point cloud following Xu et al. (2018). Finally, geometric convolution is applied.

Note that we prefer to use geometric convolution in NPTC because compared with methods that translate kernels in the ambient space of the manifold, NPTC translates kernels on the tangent planes which effectively avoids having convolution kernels defined away from the underlying manifold of the point cloud. In other words, NPTC can well reflect point cloud geometry and is a natural generalization of planar convolution in the sense that when the point cloud reduces to planar grids, the NPTC reduces to the planar convolution.

1.3 Contributions

- We introduce a new point cloud convolution, NPTC, based on parallel transport defined by a narrow-band approximation of the point cloud. The proposed NPTC is a natural generalization of planar convolution.
- The proposed NPTC combines voxelization and geometric convolution. Voxelization with appropriate resolution brings robustness and geometric convolution can better reflect point cloud's geometry.
- Based on NPTC, we designed convolutional neural networks, called NPTC-net, for point clouds classification and segmentation with state-of-the-art performance.

2 Background

2.1 Manifold and Parallel Transport

Let $\mathcal{M}$ be a 2 dimensional differential manifold embed in $\mathbb{R}^3$ and $\mathcal{T}_x\mathcal{M}$ be the tangent plane at point $x \in \mathcal{M}$. $\mathcal{T}_x\mathcal{M}$ can be defined as the 2-dimensional linear space formed by the span of 2 tangent vectors. The disjoint union of the tangent planes at each point on the manifold defines the tangent bundle $\mathcal{TM}$. A vector field $\mathbf{X}$ is a smooth assignment: $\mathcal{M} \to \mathcal{TM}$. Collection of all smooth vector fields $\mathbf{X}(x) \in \mathcal{T}_x\mathcal{M}, \forall x \in \mathcal{M}$ is denoted as $\Gamma(\mathcal{TM})$.

An affine connection is a bilinear mapping ∇: $\Gamma(\mathcal{TM}) \times \Gamma(\mathcal{TM}) \to \Gamma(\mathcal{TM})$, such that for all smooth functions f and g in $C^\infty(\mathcal{M})$ and all vector fields X, Y and z on M:

$$\begin{cases} \nabla_{fX+gY}Z = f\nabla_X Z + g\nabla_Y Z, \\ \nabla_X(aY + bZ) = a\nabla_X Y + b\nabla_X Z, \quad a, b \in \mathbb{R}, \\ \nabla_X(fY) = df(X)Y + f\nabla_X Y. \end{cases} \tag{5}$$

A section of a vector field is called **parallel** along a curve γ if $\nabla_{\dot{\gamma}}X = 0$ for $t \in I$. Suppose we are given an vector $\vec{e} \in \mathcal{T}_{x_0}$ at $x_0 = \gamma(0) \in \mathcal{M}$. The **parallel transport** of $\vec{e}$ along γ is the extension of $\vec{e}$ to a parallel section $\mathbf{X}$ on γ. More precisely, $\mathbf{X}$ is the unique section of $\Gamma(\mathcal{TM})$ along γ satisfying the ordinary differential equation $\nabla_{\dot{\gamma}(t)}\mathbf{X}(t) = 0$ with the initial value $\mathbf{X}(0) = \vec{e}$.

In differential geometry, a geodesic is a curve representing in some sense the shortest path between two points on a surface, or more generally on a Riemannian manifold. It is a generalization of the notion of a "straight line". Formally, a geodesic is $\gamma : [0, l] \to \mathcal{M}$ if $\nabla_{\dot{\gamma}(t)}\dot{\gamma}(t) = 0$.

For any two points x_0 and x_1 on $\mathcal{M}$, there will be a geodesic connecting x_0 and x_1. A geodesic on a smooth manifold $\mathcal{M}$ with an affine connection ∇ is a curve $\gamma(t)$ such that parallel transport along the curve preserves the tangent vector to the curve. That is to say, all tangential directions of one geodesic form a parallel vector field.

For convenience, instead of transporting the kernel on the manifold, we can locally construct the parallel transported kernel at every point x by formulating k as $k(\phi(x, \cdot))$, where $\phi(x, v)$ is defined in (3). It is known in differential geometry that transporting the kernel to every point on the manifold is the same as locally reconstructing the kernel in the aforementioned way.

2.2 THE EIKONAL EQUATION

The proposed NPTC relies on the computation of a distance function on a narrow-band voxel-based approximation of the given point cloud. Therefore, we review how a distance functions are calculated.

Distance functions can be easliy computed by solving the Eikonal equation. The Eikonal equation is a non-linear partial differential equation describing wave propagation:

$$|\nabla \rho| = 1/h(x), \quad x \in \Omega, \quad \rho|_{\Lambda} = 0, \tag{6}$$

where $\Lambda \subset \overline{\Omega} \subset \mathbb{R}^n$ and $f(x)$ is a strictly positive function. The solution $\rho(x)$ of (6) can be viewed as the shortest time needed to travel from x to Λ with $h(x)$ being the speed of the wave at x. For the special case when $h = 1$, the solution $\rho(x)$ represents the distance from x to Λ limited in the Ω. The Eikonal equation can be solved by the fast marching method Sethian (1996).

3 NARROWBAND PARALLEL TRANSPORT CONVOLUTION (NPTC) AND NETWORK DESIGN

Generalization of convolution defined by parallel transport on triangulated surfaces has already been proposed in Schonsheck et al. (2018). In this section, we discuss how to transport kernels on point clouds in a similar fashion.

3.1 NARROWBAND PARALLEL TRANSPORT CONVOLUTION (NPTC)

Given a function $f : \mathcal{P} \to \mathbb{R}$, the NPTC of f with kernel k takes the same form as (2). Under such formulation, the key to design a convolution is to design vector fields $\{\vec{u}_x^j\}_{x \in \mathcal{M}}$, $j, = 1, 2$. In this subsection, we discuss the general idea of NPTC and the interpretation of it in terms of parallel transport.

3.1.1 GENERAL IDEA OF NPTC

To select a suitable vector field, we first recall the choice of the vector fields of PTC which defines convolution on triangulated surfaces via parallel transport with respect to the Levi-Civita connection Schonsheck et al. (2018). Geodesic curve represents, in some sense, the shortest path between two points on a Riemannian manifold. Given a geodesic connecting two points x and y, the tangential direction at x corresponds to the ascend direction of geodesic distance from y. PTC chooses such direction as $\vec{u}_x^1$ and defines $\vec{u}_x^2 = \vec{u}_x^1 \times \vec{n}_x$ with $\vec{n}_x$ the normal vector at x.

If we want to construct a vector field on point cloud, gradients of some sort of distance function can be a good choice. However, unlike triangulated surfaces, distance function is not easily defined on point clouds due to the lack of connectivity. It is then natural to approximate the point cloud with another data structure with connectivity, so that distance function can be easily calculated. We use voxelization Wu et al. (2015) to approximate the point cloud in a narrow-band in $\mathbb{R}^3$ covering the point cloud. We denote such distance function as $\rho : \mathbb{R}^3 \to \mathbb{R}^+$. We will elaborate how ρ can be calculated in later parts of this subsection.

Note that if the point cloud is sampled from a plane, the narrow-band is flat as well. Then, by a proper choice of the distance function, the vector fields $\{\vec{u}_x^j\}_{x \in \mathcal{M}}, j = 1, 2$, can be reduced to the global coordinate $\{\vec{e}_j\}, j = 1, 2$ on the plane. This means that NPTC is reduced to the traditional planar convolution.

Once the distance function ρ is computed, we choose $\vec{u}_x^1 = \nabla_{\mathcal{P}} \rho(x)$, where $\nabla_{\mathcal{P}} \rho(x)$ is a projection of $\nabla \rho(x)$ on an approximated tangent plane at x. Then, $\vec{u}_x^2$ can be calculated by the outer product $\vec{u}_x^2 = \vec{u}_x^1 \times \vec{n}_x$ with $\vec{n}_x$ the normal vector at x. The value $f(v)$ is computed by $f(v) = f(z)$ where $z \in \mathcal{P}$ is the closest point to v. Note that one may use a more sophisticated method to compute $f(v)$ rather than using the closest point interpolation. We choose the closest point interpolation because of its simplicity.

We finally note that NPTC defined by the aforementioned way indeed defines certain parallel transport convolution. In fact, by given smooth vector fields $\{\vec{u}^1, \vec{u}^2\}$, we can define linear transformation among tangent planes $\mathcal{L}(\gamma)_s^t : \mathcal{T}_{\gamma(s)}\mathcal{M} \to \mathcal{T}_{\gamma(t)}\mathcal{M}$, then the corresponding parallel transport

through the associated infinitesimal connection $\nabla_{\dot{\gamma}} V = \lim_{h \to 0} \frac{1}{h}(\mathcal{L}(\gamma)_0^h(V_{\gamma(0)}) - V_{\gamma(0)})$ can be induced Knebelman (1951). Therefore, convolution defined by NPTC can be viewed as parallel transporting the kernels on the manifold with respect to the connection that is reconstructed from the vector field $\{\vec{u}_x^1\}_{x \in \mathcal{M}}$.

3.1.2 Computing Distance Function on Point Clouds

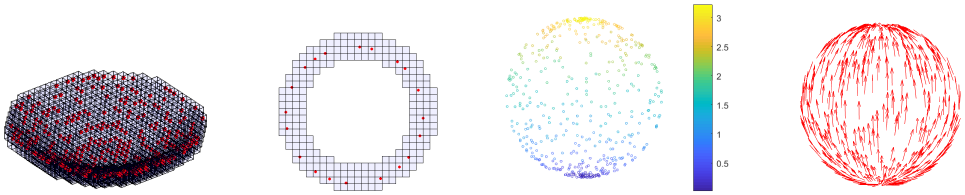

(a) narrow-band (b) cross section (c) Distance function ρ (d) $\{\vec{u}_x^1\}$

Figure 2: Illustration of a point cloud $\mathcal{P}$ sampled from the unit sphere. (a) shows the narrow-band approximation (blue boxes) of part of $\mathcal{P}$ (in red). (b) is a cross section of (a). (c), (d) show the distance function ρ and vector field $\{\vec{u}_x^1\}$ ($\{\nabla_{\mathcal{P}} \rho(x)\}$) on the point cloud. We can see that distance propagates from the bottom center to the top center reflecting the geometry of the sphere.

For simplicity, we consider point clouds in $\mathbb{R}^3$ in this subsection, though the arguments is also valid in $\mathbb{R}^n$. A point cloud is entirely discrete without inherent connectivity. Therefore, it is not straightforwardly compute distance function on point clouds although the local mesh method Lai et al. (2013) can be applied to solve the Eikonal equation. For simplicity, we use voxels to approximate point clouds and to compute distance functions on the voxels using the well-known fast marching method based on regular grid provided by the voxelization Sethian (1996). Note that, using voxels to compute distance functions is fast and robust to noise and local deformations.

The solution $\rho(x)$ of the Eikonal equation $|\nabla \rho(x)| = 1$ presents the distance form Λ to x limited inside the narrow-band. Here Λ is chosen as certain point on the point cloud.

Although generating multiple vector fields by selecting different starting points is helpful to eliminate singularities, experiments show that the directly selecting one point already provides satisfactory results. Finally, we interpolate the distance function from the voxels to point cloud.

3.1.3 Computing the Vector Fields on Point Clouds

We first compute the tangent plane on each point. Tangent planes are important features of manifolds and have been well-studied in the literature Lai et al. (2013). In this paper, we use local principal component analysis (LPCA) to estimate the tangent plane. We estimate the local linear structure near $x \in \mathcal{P}$ using the covariance matrix

$$\sum_{x_k \in \mathcal{N}(x)} (x_k - c)^\top (x_k - c), \quad c = \frac{1}{k} \sum_{x_k \in \mathcal{N}(x)} x_k,$$

where $\mathcal{N}(x)$ is the set of neighboring points of x. The eigenvectors of the covariance matrix form an orthogonal basis. If the point cloud is sampled from a two dimensional manifold, and the local sampling is dense enough to resolve local features, the eigenvectors corresponding to the largest two eigenvalues provide the two orthogonal directions of the tangent plane, and the remaining vector represents the normal direction at $x \in \mathcal{P}$. Here, we denote the space spanned by the two eigenvectors of the covariance matrix at x as $\mathcal{T}_x \mathcal{P} \subset \mathbb{R}^3$.

With the computed distance function $\rho(x)$, it is nature to define the vector field by projecting $\nabla \rho$ on the approximated tangent planes of the point cloud. Given a point $x_k \in \mathcal{P}$ close enough to $x \in \mathcal{P}$, we have

$$\langle \nabla \rho, x_k - x \rangle \approx \rho(x_k) - \rho(x),$$

where $\rho(x_k)$ and $\rho(x)$ are known. If we consider k-nearest neighbors of x, we have $k-1$ equations with 3 unknowns that are the three components of $\nabla \rho$. We can use least squares to find $\nabla \rho$. We then project the vector $\nabla \rho(x)$ onto the tangent plane at x. We denote the projected vector $\nabla_{\mathcal{P}} \rho$, which is the vector we eventually need to define NPTC as described in Section 3.1.1.

3.2 NPTC-NET: ARCHITECTURE DESIGN FOR CLASSIFICATION AND SEGMENTATION

This section, we present how to use NPTC to design convolutional neural networks on point clouds for classification and segmentation tasks. For that, other than the NPTC, we need to define some other operations that are frequently used in neural networks. Note that, some point-wise operations like MLP and ReLu are the same on point cloud as the Euclidean case. Here, we only focus on the operations that are not readily defined on point clouds.

Down-sampling: In our implement, the sub-sampled set of points of the next layer is generated by the farthest point sampling Eldar et al. (1997).

Convolution layer: Our k-th convolution layer takes points $\mathcal{P}^k \in \mathbb{R}^{N^k \times 3}$ and their corresponding feature maps $\mathcal{F}^k \in \mathbb{R}^{N^k \times c^k}$ as input, where N^k is the number of the points and c^k is the number of channels at layer k. The corresponding output is $\mathcal{F}^{k+1} \in \mathbb{R}^{N^{k+1} \times c^{k+1}}$ living on the points $\mathcal{P}^{k+1} \in \mathbb{R}^{N^{k+1} \times 3}$. The NPTC-net have encoding and decoding stages. Normally, $N^{k+1} < N^k$ during encoding and $N^k < N^{k+1}$ during decoding. Convolution at the k-th layer is only performed on the point set $\mathcal{P}^{k+1}$, which resembles convolution with stride > 1 for planar convolutions.

Residual block: One residual block takes the feature maps $\mathcal{F} \in \mathbb{R}^{N \times c}$ on the point set $\mathcal{P} \in \mathbb{R}^{N \times 3}$ as input and same number of points and same number of channels of features as output. One residual layer consists of three components: MLP from c channels to $\frac{c}{2}$ channels, convolution layer from $\frac{c}{2}$ channels to $\frac{c}{2}$ channels, MLP from $\frac{c}{2}$ channels to c channels plus the feature maps from the bypass connection. A residual block consists of several residual layers.

NPTC-net consists of the aforementioned operations and its architecture is given by Figure 3. The left half of the NPTC-net is the encoder part of the network for feature extraction. For classification, features at the bottom of the network are directly attached to a classification network; while for segmentation, features are decoded using the right half of the NPTC-net (decoder part of the network) to output the segmentation map.

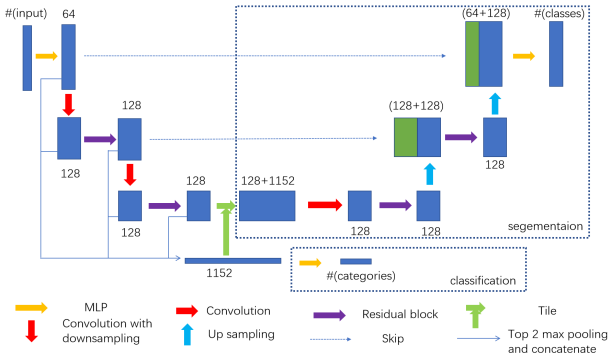

Figure 3: Architecture of NPTC-net. Top 2 max pooling means taking the maximum two values among all the points in each channel and then concatenate into one vector representing global feature. "Tile" means repeating the global feature and concatenating to each point as extra channels.

4 EXPERIMENTS

In order to evaluate our new NPTC-nets, we conduct experiments on three widely used 3D datasets, ModelNet Wu et al. (2015), ShapeNet Yi et al. (2016), S3DIS Armeni et al. (2016). We implement the model on a GTX TITAN Xp GPU. For more implementation details, please refer to Appendix.

4.1 3D SHAPE CLASSIFICATION AND SEGMENTATION

We test the NPTC-net on ModelNet40 for classification tasks. ModelNet40 contains 12,311 CAD models from 40 categories with 9,842 samples for training and 2,468 samples for testing. For comparison, we use the data provided by Qi et al. (2017a) sampling 2,048 points uniformly and computing the normal vectors from the mesh. As shown on Tabel 1, our networks outperform other

state-of-art methods. (If a compared method has results on both 2048 (or 1024) and 5000 points, we only compare with the former.).

We also evaluate the NPTC-net on ShapeNet Part for segmentation tasks. ShapeNet Part contains 16,680 models from 16 shape categories with 14,006 for training and 2,874 for testing, each annotated with 2 to 6 parts and there are 50 different parts in total. We follow the experiment setup of previous works, putting object category into networks as known information. We use point intersection-over-union (IoU) to evaluate our NPTC-net. Table 1 shows that our model ranks second on this dataset and is fairly close to the best known result.

Table 1: Comparisons of overall accuracy (OA) and mean per-class accuracy (mA) on ModelNet40 as well as comparisons in instance average IoU (mIoU) and class average IoU (mcIoU) on ShapeNet Part. Models ranking first is colored in red and second in blue.

	Modelnet40		ShapeNet part	
Method	OA(%)	mA(%)	mIoU	mcIoU
kd-net Klokov & Lempitsky (2017)	91.8	88.5	82.3	77.4
pointnet Qi et al. (2017a)	89.2	86.2	83.7	80.4
SO-Net Li et al. (2018a)	90.9	87.3	84.9	81.0
pointnet++ Qi et al. (2017b)	90.7	-	85.1	81.9
SpecGCN Wang et al. (2018a)	92.1	-	85.4	-
SpiderCNN Xu et al. (2018)	92.4	-	85.3	81.7
pointcnn Li et al. (2018b)	92.2	88.1	86.1	84.6
DGCNN Wang et al. (2018c)	92.2	90.2	85.1	82.3
Ours	92.7	90.2	85.8	83.3

4.2 RUBOSTNESS TEST

As pointed out earlier, using voxelization can bring rubustness to the definition of geometric convolution. In order to show the robustness of our model for real data, we tested scene semantics segmentation on the "Stanford Large-Scale 3D Indoor Spaces Dataset" (S3DIS). S3DIS covers six large-scale indoor areas from 3 different buildings for a total of 273 million points annotated with 13 classes. This is a real-word scanned dataset without normal and with noise. Following Tchapmi et al. (2017), we advocate the use of Area-5 as test scene to better measure the generalization ability of our method. Table 2 shows that geometric convolution methods are close to the methods which do not need normal estimation. NPTC-net outperforms the best known geometric convolution method TangentConvXu et al. (2018).

Table 2: Comparisons of overall accuracy (OA) and mean per-class IoU (mIoU) on S3DIS. Models ranking first is colored in red and second in blue.

Convolution Type	Method	OA(%)	mIoU(%)
no convolution	pointnet Qi et al. (2017a)	78.8	41.3
3-d convolution	SegCloud Tchapmi et al. (2017)	-	48.9
	Eff3DConvZhang et al. (2018)	69.3	51.8
	ParamConvWang et al. (2018b)	-	58.3
geometric convolution	TangentConv Xu et al. (2018)	82.5	52.8
	Ours	83.7	54.0

5 CONCLUSION

This paper proposed a new way of defining convolution on point clouds, called the narrow-band parallel transport convolution (NPTC), based on a point cloud discretization of a manifold parallel transport. The parallel transport was defined specifically by a vector field generated by the gradient field of a distance function on a narrow-band approximation of the point cloud. The NPTC was used to design a convolutional neural network (NPTC-net) for point cloud classification and segmentation. Comparisons with state-of-the-art methods indicated that the proposed NPTC-net is competitive with the best existing methods.

REFERENCES

I. Armeni, O. Sener, A. R. Zamir, H. Jiang, I. Brilakis, M. Fischer, and S. Savarese. 3d semantic parsing of large-scale indoor spaces. In *2016 IEEE Conference on Computer Vision and Pattern Recognition (CVPR)*, pp. 1534–1543, Los Alamitos, CA, USA, jun 2016. IEEE Computer Society. doi: 10.1109/CVPR.2016.170. URL https://doi.ieeecomputersociety.org/10.1109/CVPR.2016.170.

Davide Boscaini, Jonathan Masci, Emanuele Rodolà, and Michael Bronstein. Learning shape correspondence with anisotropic convolutional neural networks. In D. D. Lee, M. Sugiyama, U. V. Luxburg, I. Guyon, and R. Garnett (eds.), *Advances in Neural Information Processing Systems 29*, pp. 3189–3197. Curran Associates, Inc., 2016. URL http://papers.nips.cc/paper/6045-learning-shape-correspondence-with-anisotropic-convolutional-neural-networks.pdf.

M. M. Bronstein, J. Bruna, Y. LeCun, A. Szlam, and P. Vandergheynst. Geometric deep learning: Going beyond euclidean data. *IEEE Signal Processing Magazine*, 34(4):18–42, July 2017. ISSN 1053-5888. doi: 10.1109/MSP.2017.2693418.

Joan Bruna, Wojciech Zaremba, Arthur Szlam, and Yann Lecun. Spectral networks and locally connected networks on graphs. In *International Conference on Learning Representations (ICLR2014), CBLS, April 2014*, 2014.

Michaël Defferrard, Xavier Bresson, and Pierre Vandergheynst. Convolutional neural networks on graphs with fast localized spectral filtering. In D. D. Lee, M. Sugiyama, U. V. Luxburg, I. Guyon, and R. Garnett (eds.), *Advances in Neural Information Processing Systems 29*, pp. 3844–3852. Curran Associates, Inc., 2016. URL http://papers.nips.cc/paper/6081-convolutional-neural-networks-on-graphs-with-fast-localized-spectral-filterin pdf.

Bin Dong. Sparse representation on graphs by tight wavelet frames and applications. *Applied and Computational Harmonic Analysis*, 42(3):452 – 479, 2017. ISSN 1063-5203. doi: https://doi.org/10.1016/j.acha.2015.09.005. URL http://www.sciencedirect.com/science/article/pii/S1063520315001372.

Yuval Eldar, Michael Lindenbaum, Moshe Porat, and Yehoshua Y Zeevi. The farthest point strategy for progressive image sampling. *IEEE Transactions on Image Processing*, 6(9):1305–1315, 1997.

Ian Goodfellow, Yoshua Bengio, and Aaron Courville. *Deep learning*. MIT press, 2016.

David K. Hammond, Pierre Vandergheynst, and Rmi Gribonval. Wavelets on graphs via spectral graph theory. *Applied and Computational Harmonic Analysis*, 30(2):129 – 150, 2011. ISSN 1063-5203. doi: https://doi.org/10.1016/j.acha.2010.04.005. URL http://www.sciencedirect.com/science/article/pii/S1063520310000552.

R. Klokov and V. Lempitsky. Escape from cells: Deep kd-networks for the recognition of 3d point cloud models. In *2017 IEEE International Conference on Computer Vision (ICCV)*, pp. 863–872, Los Alamitos, CA, USA, oct 2017. IEEE Computer Society. doi: 10.1109/ICCV.2017.99. URL https://doi.ieeecomputersociety.org/10.1109/ICCV.2017.99.

MS Knebelman. Spaces of relative parallelism. *Annals of Mathematics*, pp. 387–399, 1951.

Rongjie Lai, Jiang Liang, and Hongkai Zhao. A local mesh method for solving pdes on point clouds. *Inverse Prob. and Imaging*, 7(3):737–755, 2013.

Yann LeCun, Yoshua Bengio, and Geoffrey Hinton. Deep learning. *nature*, 521(7553):436, 2015.

R. Levie, F. Monti, X. Bresson, and M. M. Bronstein. Cayleynets: Graph convolutional neural networks with complex rational spectral filters. *IEEE Transactions on Signal Processing*, 67(1):97–109, Jan 2019. ISSN 1053-587X. doi: 10.1109/TSP.2018.2879624.

Jiaxin Li, Ben M. Chen, and Gim Hee Lee. So-net: Self-organizing network for point cloud analysis. In *The IEEE Conference on Computer Vision and Pattern Recognition (CVPR)*, June 2018a.

Yangyan Li, Rui Bu, Mingchao Sun, Wei Wu, Xinhan Di, and Baoquan Chen. Pointcnn: Convolution on x-transformed points. In S. Bengio, H. Wallach, H. Larochelle, K. Grauman, N. Cesa-Bianchi, and R. Garnett (eds.), *Advances in Neural Information Processing Systems 31*, pp. 820–830. Curran Associates, Inc., 2018b. URL http://papers.nips.cc/paper/7362-pointcnn-convolution-on-x-transformed-points.pdf.

Jonathan Masci, Davide Boscaini, Michael M. Bronstein, and Pierre Vandergheynst. Geodesic convolutional neural networks on riemannian manifolds. In *The IEEE International Conference on Computer Vision (ICCV) Workshops*, December 2015.

Charles R. Qi, Hao Su, Kaichun Mo, and Leonidas J. Guibas. Pointnet: Deep learning on point sets for 3d classification and segmentation. In *The IEEE Conference on Computer Vision and Pattern Recognition (CVPR)*, July 2017a.

Charles Ruizhongtai Qi, Li Yi, Hao Su, and Leonidas J Guibas. Pointnet++: Deep hierarchical feature learning on point sets in a metric space. In I. Guyon, U. V. Luxburg, S. Bengio, H. Wallach, R. Fergus, S. Vishwanathan, and R. Garnett (eds.), *Advances in Neural Information Processing Systems 30*, pp. 5099–5108. Curran Associates, Inc., 2017b. URL http://papers.nips.cc/paper/7095-pointnet-deep-hierarchical-feature-learning-on-point-sets-in-a-metric-space.pdf.

Stefan C. Schonsheck, Bin Dong, and Rongjie Lai. Parallel transport convolution: A new tool for convolutional neural networks on manifolds. *CoRR*, abs/1805.07857, 2018. URL http://arxiv.org/abs/1805.07857.

James A Sethian. A fast marching level set method for monotonically advancing fronts. *Proceedings of the National Academy of Sciences*, 93(4):1591–1595, 1996.

Maxim Tatarchenko, Jaesik Park, Vladlen Koltun, and Qian-Yi Zhou. Tangent convolutions for dense prediction in 3d. In *The IEEE Conference on Computer Vision and Pattern Recognition (CVPR)*, June 2018.

L. Tchapmi, C. Choy, I. Armeni, J. Gwak, and S. Savarese. Segcloud: Semantic segmentation of 3d point clouds. In *2017 International Conference on 3D Vision (3DV)*, pp. 537–547, Oct 2017. doi: 10.1109/3DV.2017.00067.

Chu Wang, Babak Samari, and Kaleem Siddiqi. Local spectral graph convolution for point set feature learning. In *The European Conference on Computer Vision (ECCV)*, September 2018a.

Shenlong Wang, Simon Suo, Wei-Chiu Ma, Andrei Pokrovsky, and Raquel Urtasun. Deep parametric continuous convolutional neural networks. In *Proceedings of the IEEE Conference on Computer Vision and Pattern Recognition*, pp. 2589–2597, 2018b.

Yue Wang, Yongbin Sun, Ziwei Liu, Sanjay E. Sarma, Michael M. Bronstein, and Justin M. Solomon. Dynamic graph CNN for learning on point clouds. *CoRR*, abs/1801.07829, 2018c. URL http://arxiv.org/abs/1801.07829.

Wenxuan Wu, Zhongang Qi, and Fuxin Li. Pointconv: Deep convolutional networks on 3d point clouds. *CoRR*, abs/1811.07246, 2018. URL http://arxiv.org/abs/1811.07246.

Zhirong Wu, Shuran Song, Aditya Khosla, Fisher Yu, Linguang Zhang, Xiaoou Tang, and Jianxiong Xiao. 3d shapenets: A deep representation for volumetric shapes. In *The IEEE Conference on Computer Vision and Pattern Recognition (CVPR)*, June 2015.

Yifan Xu, Tianqi Fan, Mingye Xu, Long Zeng, and Yu Qiao. Spidercnn: Deep learning on point sets with parameterized convolutional filters. In *The European Conference on Computer Vision (ECCV)*, September 2018.

Li Yi, Vladimir G. Kim, Duygu Ceylan, I-Chao Shen, Mengyan Yan, Hao Su, Cewu Lu, Qixing Huang, Alla Sheffer, and Leonidas Guibas. A scalable active framework for region annotation in 3d shape collections. *ACM Trans. Graph.*, 35(6):210:1–210:12, November 2016. ISSN 0730-0301. doi: 10.1145/2980179.2980238. URL http://doi.acm.org/10.1145/2980179.2980238.

Chris Zhang, Wenjie Luo, and Raquel Urtasun. Efficient convolutions for real-time semantic segmentation of 3d point clouds. In *2018 International Conference on 3D Vision (3DV)*, pp. 399–408. IEEE, 2018.

A APPENDIX

A.1 IMPLEMENTATION DETAILS

We implement the model with Tensorflow using SGD optimizer with an initial learning rate 0.1 for ModelNet40 and ADAM optimizer with an initial learning rate 0.002 for ShapeNet Part and S3DIS on a GTX TITAN Xp GPU. During the training procedure of classification, the data is augmented by random rotation, scaling and Gaussian perturbation on the coordinates of the points. During the training procedure of segmentation, the data is augmented by scaling and Gaussian perturbation on the coordinates of the points.

Following Li et al. (2018b), the data of S3DIS is firstly split by room, and then the rooms are sliced into 1.5m by 1.5m blocks, with 0.3m padding on each side. The points in the padding areas serve as context of the internal points, and themselves are not linked to loss in the training phase, nor used for prediction in the testing phase. Each block will be viewed as a point cloud during training and testing.

We do inferences on the augmented data during testing by voting following Qi et al. (2017b). To clarify this, let x^i be one data from the test set and x^i_j be the augmented data generated from x^i. $p^i_j = f(x^i_j)$ denotes the predict possibility vector after Softmax. The final inference result of x^i is $\text{Predict}(x^i) = \arg\max_k (\sum_j p^i_j)_k$.

A.2 RUNNING STATISTICS

Table 3: Comparisons of number of parameters and FLOPs for classification.

method	Parameters	FLOPs(Inference)
pointnet Qi et al. (2017a)	3.48M	14.70B
pointnet++ Qi et al. (2017b)	1.48M	26.94B
DGCNN Wang et al. (2018c)	1.84M	44.27B
pointcnn Li et al. (2018b)	**0.6M**	25.30B
Ours	1.29M	**11.7B**

Table 4: Comparisons of training time of networks on ModelNet40

Method	Settings	Accuracy and Training (+Pre-processing) time
PointNet++ Qi et al. (2017b)	adam, 1024 points	90.7%, 6 hours
	adam, 5000 points	91.9%, 20 hours
ours	adam, 2048 points	92.4%, 6h (+1.5h)
	SGD, 2048 points	92.7%, 12h (+1.5h)

As shown in Table 3, we summarize our running statistics based with model for ModelNet40 with batch size 16. In comparison with several other methods, although we use ResNet structure, the fewer channels, smaller kernels and simpler interpolation (nearest neighboring) make NPTC use similiar parameters and even fewer FLOPs.

Total pre-processing time mainly depends on the grid's density. For most cases, the resolution of 100^3 is enough to describe the shape of the point cloud, which is what we chose for our experiments. We also remark that the whole computation cost of constructing convolution is linearly depending on the resolution of voxel and the size of data. On a PC with Core i7-7700 CPU, the pre-processing takes about **0.5** seconds per point cloud with Matlab, and the whole dataset of ModelNet40 (12,311 shapes with 10,000 points each) takes only about 1.5 hours. It is negligible compared to the training of the deep neural networks and acceptable to do inference in practice.

A.3 VISUALIZATION

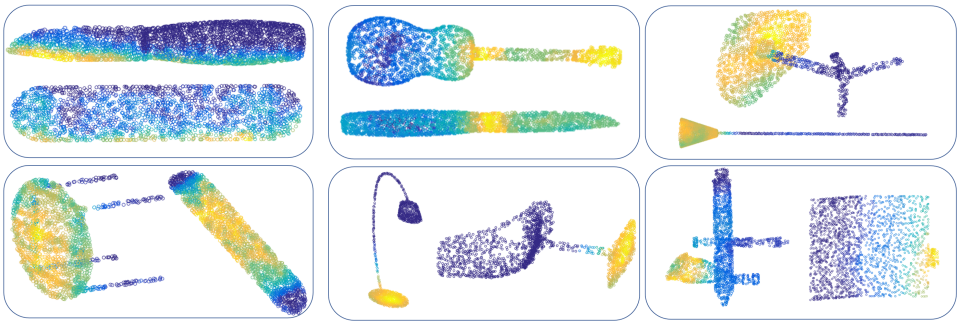

(a) low-level features (b) high-level features

Figure 4: Feature Visualization: each feature from low or high level is displayed on 2 point clouds from different categories. High-level activations are in yellow and low-level activations are in blue.

To visualize the effects of the proposed NPTC in the NPTC-net, we trained the network on ShapeNet Part and visualize learned features by coloring the points according to their level of activation. In Figure 4, filters from the the first Convolution layer in the the first Residual block and final Convolution layer in the second Residual block are chosen. In order to easily compare the features at different levels, we interpolate them on the input point cloud. Observe that low-level features mostly represent simple structures like edges (top of (a)) and planes (bottom of (a)) with low variation in their magnitudes. In deeper layers, features are richer and more distinct from each other, like bottleneck (upper left of (b)), ”big-head”(upper right of (b)), plane base (lower left of (b)), bulge (lower right of (b)).